metals

MDPI

Article

Corrosion Behavior of Nickel–Titanium Continuous-Casted Alloys

Minja Miličić Lazić [1], Dijana Mitić [1], Katarina Radović [1], Igor Đorđević [1], Peter Majerič [2], Rebeka Rudolf [2] and Branimir N. Grgur [3,*]

[1] School of Dental Medicine, University of Belgrade, 11000 Belgrade, Serbia; minja.milicic@stomf.bg.ac.rs (M.M.L.); dijana.trisic@stomf.bg.ac.rs (D.M.); katarina.radovic@stomf.bg.ac.rs (K.R.); igor.djordjevic@stomf.bg.ac.rs (I.Đ.)
[2] Faculty of Mechanical Engineering, University of Maribor, 2000 Maribor, Slovenia; peter.majeric@um.si (P.M.); rebeka.rudolf@um.si (R.R.)
[3] Faculty of Technology and Metallurgy, University of Belgrade, 10200 Belgrade, Serbia
* Correspondence: bngrgur@tmf.bg.ac.rs

Abstract: Variations in the corrosion behavior of biomedical NiTi alloys in Cl^- containing and acidic environments present a problem with their biological implantation. The objective of this research was to evaluate the synergy of the microstructure, the corrosion behavior, and the biocompatibility of novel continuous-cast NiTi alloys and to compare them with commercial NiTi alloys. The two alloys have a practically identical nominal chemical composition, but they differ in production technology. The continuous casting technology involved vacuum induction melting of the basic components and vertical continuous casting, while the commercial NiTi alloy was produced through a process of casting, hot rolling, and forming into square shapes. The microstructure was revealed to determine the surface area and size of grains. The corrosion of a commercial nickel–titanium alloy and one prepared by a novel continuous casting method in acidic and chloride-containing solutions was studied via analytical and electrochemical tests. Localized corrosion characteristics related to oxide properties, when exposed to 9 g L^{-1} NaCl solution, were examined with focused ion beam analysis and subsequent microchemical analysis of the formed corrosive products. Corrosion potential over time and the oxide film resistance were analyzed using linear polarization measurements. To obtain a preliminary estimate of biocompatibility, human fibroblast cells were used in indirect contact, i.e., alloy conditioning medium. The continuous casting method resulted in a reduction in the average grain size in comparison to the commercial sample and better corrosion stability of the sample in an acidic environment. Also, in a solution of 9 g L^{-1} NaCl the commercial sample showed high values for the corrosion current density (j_{corr} = 6 μA cm^{-2}), which indicated low corrosion resistance, while the continuous casting sample possessed much better corrosion stability and lower values for the corrosion current density (j_{corr} = 0.2 μA cm^{-2}). In line with that, elemental analysis of the corroded surfaces showed higher Cl^- ion deposition over the surface layer of the commercial sample, suggesting local oxide breakdown. Moreover, $NiTi_{cc}$ reached a value three times higher for polarization resistance (R_p = 270 kΩ cm^2) over time in comparison to the commercial sample (R_p~100 kΩ cm^2). Biocompatibility evaluation showed that human fibroblast cells exhibited altered metabolic activity. An MTT assay showed that cells' mitochondrial activity dropped below that of control cells in the presence of both materials' supernatants.

Keywords: nickel–titanium; corrosion behavior; electrochemical testing; NiTi biocompatibility

Citation: Lazić, M.M.; Mitić, D.; Radović, K.; Đorđević, I.; Majerič, P.; Rudolf, R.; Grgur, B.N. Corrosion Behavior of Nickel–Titanium Continuous-Casted Alloys. *Metals* **2024**, *14*, 88. https://doi.org/10.3390/met14010088

Academic Editor: Youngsik Kim

Received: 27 October 2023
Revised: 13 December 2023
Accepted: 28 December 2023
Published: 11 January 2024

1. Introduction

Among different shape memory alloys (SMAs), nickel–titanium has favorable properties that guarantee good mechanical compatibility with biological tissues. The properties of nitinol that suit its application in medicine and dentistry are good biocompatibility,

corrosion resistance, superelasticity, and fatigue resistance. The main disadvantage of Ti-based, nickel-free SMAs is the low critical stress for slip deformation. Consequently, those nickel-free SMAs have lower recoverable strain and functional stability. Only NiTi alloys are capable of recovering inelastic strains up to 8%. Additionally, NiTi SMAs have a lower Young's modulus in comparison to Ti-based SMAs, and thus better mechanical compatibility with osseous tissue, as seen in [1,2]. Considering a wide range of medical applications, the corrosion resistance of nitinol medical devices is a crucial factor in defining their biocompatibility [3]. The corrosion of nickel–titanium alloys is contextual, depending on different environmental (extrinsic) and material-related (intrinsic) variables. Variations in chemical composition, surface treatments, microstructure, and passive film thickness play significant roles in preventing metal ion leaching. Regarding the nature of the environment, the human body presents very challenging surroundings [4]. The reason for that is the presence of dissolved oxygen, chlorides, and changes in pH levels (acid–base disbalance). Moreover, different parts of the human body vary significantly depending on the oxygen concentrations and pH values.

Various studies have demonstrated the lower corrosion resistance of these alloys in chloride-containing environments, such as [5,6], and acidic solutions, as it is well documented that the corrosion potential increases as the pH value decreases [7].

Nickel–titanium alloys are known for their passivation state when exposed to oxygen. The problem with different chloride-containing environments for passive alloys is that these most aggressive halide ions will lead to oscillations in the passive region, so-called metastable pitting. Regarding the easy adsorption of chloride ions, the initiation of pitting corrosion will occur. The pits are characterized by a high concentration of metal and hydrogen cations because of the hydrolysis reaction [1]. Both hydrogen and chloride ions encourage metal dissolution, and the pit propagates due to pH reduction within the pit. This phenomenon is also known as the "local acidification mechanism" [8]. Regarding the fact that the local decrease in pH values is the primary factor affecting localized corrosion, these conditions will support further propagation of pitting corrosion. Once the halide ions reach the metal/oxide interface, the breakdown mechanism will take place, provoking pit propagation and accelerated dissolution of the alloys [9].

Metal's ability to recover, i.e., repassivate, also depends on the dissolved oxygen levels in the body's fluids. Due to the combination of hemoglobin, the partial oxygen pressure in blood is between 40 (venous) and 100 (arterial) mm Hg, which is less than the partial oxygen in the air (approximately 160 mm Hg) [10]. This fact creates more challenging conditions for the recovery of the oxide layer after the attack of other corrosion agents. Other disturbing factors in human blood are bicarbonate salts (i.e., rapid-acting chemical buffers) and CO_2, resulting in more H^+ ions and a lower pH [1,11]. For example, during dental implant placement, the surgical site is characterized by these challenging conditions for approximately 2 weeks [12]. Therefore, it is clear that those conditions are not only challenging but also demanding when performing experiments in in vitro conditions.

However, the above-mentioned concerns are related to nitinol devices with compromised surface finishing characteristics. The surface characteristics of NiTi alloys are highly dependent on the preparation method. NiTi alloy manufacturing is usually very demanding. Titanium has a high melting point, low fluidity (high viscosity), and a susceptibility to oxidization at high temperatures. These properties make it and its alloys difficult to cast. All NiTi alloys go through similar steps of fabrication. These steps are melting (vacuum melting techniques), forming, secondary processing methods, and finishing techniques. Commercially available NiTi alloys are now manufactured using a classical casting method that produces large blocks of solidified NiTi alloys, which are then difficult to prepare (special tools are needed) for further operations, with which alloys gain some functional properties. With continuous casting, it is possible to obtain an NiTi alloy in just one step, which would have similar properties to that which is already on the market. Continuous casting is a manufacturing process where molten metal is solidified into a semi-finished product [13]. Metal is melted in the crucible and then cast through a mold. The casting

travels downwards and its length increases with time. Continuous casting is characterized by high cooling rates which allow a very short time for the diffusion processes and can lead to an extremely fine microstructure that increases the material's toughness.

Literature-based evidence is coherent about the statement that the Ni/Ti ratio on the surface can vary significantly [14]. Also, during exposure to a corrosive environment, the thickness of the oxide on the surface of a nickel–titanium alloy can be in a wide range on the nanometer scale, from 4 nm to 3500 nm [15]. Several studies have analyzed the oxide layer growth potential on a sample's surface [16]. Results showed that untreated samples developed a thicker oxide on the surface (120–340 nm), while on mechanically polished or etched samples, the film is up to 10 times thinner (11–16 nm) [17]. However, the protective role of the surface oxide layer against corrosive agents is determined by the ability of the alloy to develop a homogeneous and compact oxide. The integrity of this layer is much more important than its thickness [18].

To date, various surface treatments have been investigated. The most common are traditional methods, which include mechanical polishing, electrochemical polishing, chemical etching in acid solutions, and heat treatment (treatment in an autoclave) [19]. In addition, there are plasma ion implantation methods and bioactive coating formation [14]. In the early 1980s, in vitro studies reported that hot and cold working processes (i.e., secondary production processes) change the inner structure and the grain size leading to surface heterogeneity. In addition to grain deformation, these procedures may break down the passive surface layer [4].

The literature is humble with evidence of the corrosion properties of NiTi alloys in cast conditions, as these characteristics are mostly studied after annealing at different times and temperatures. The importance of the biological characterization of semi-finished products can result in time- and cost-effectiveness [20].

This paper reflects the corrosion resistance of NiTi alloys covering acidic and chloride-containing solutions. The study aimed to examine how a novel method of continuous casting affects microstructure and surface chemical stability, leading to better homogeneity of the protective oxide layer. Also, the biocompatibility of the investigated alloy is examined.

2. Materials and Methods

2.1. Processing of the Samples

Nickel titanium alloy (obtained with two different casting methods, and both met the requirements prescribed by the ASTM F2063-18 (Standard Specification for Wrought Nickel-Titanium Shape Memory Alloys for Medical Devices and Surgical Implants) employed in dental devices was chosen for this study. Nickel–titanium alloy was produced by vacuum induction melting (Leybold Hereaeus, Helsinki, Finland), followed by a novel continuous casting method (denoted as $NiTi_{cc}$, composition 53.58 at.% of nickel, 46.42 at.% of titanium), with a laboratory scale vertical continuous casting (VCC) device (Technica Guss). Specifications of the laboratory VCC device are accessible in previous publications [21,22]. The corrosion behavior of continuous-cast alloy was compared with that of commercial nitinol (NiTi as cast, composition 50 at.% of nickel, 50 at.% of titanium, manufactured by the classical process, i.e., from remelting in a vacuum furnace with electro-resistive heating and final casting into ingots (Merkur d.d, Celje, Slovenija)).

2.2. Microstructure Observation and ASTM Analysis—Grain Size Measurements

In order to identify microstructural features, the samples were prepared according to the protocol for metallographic preparation: grinding, polishing with an Al_2O_3 suspension of 1 µm, and cleaning with deionized water in ultrasound. The prepared surface was chemically etched with 3 mL HF, 6 mL HNO_3, and 100 mL of water for 30 s. and observed on Nikon Epiphot 300 (Nikon, Tokio, Japan) device. Based on the fact that nickel–titanium alloys belong to multiphase systems, the plain method (real counting of grains in a given area) was used to determine the grain size of NiTi as cast and $NiTi_{cc}$. The number of grains per unit area, NA, was used to determine the grain number—G according to ASTM—using

Soft Imaging System (AnalySIS, 2002, Munster, Germany). The accuracy of this method was in counted grains.

2.3. Corrosion Testing

Before each corrosion test, sample surfaces were prepared by polishing with SiC paper (1000–4000 grit). After that, the samples were ultrasonically cleaned in ethanol and deionized water.

2.3.1. Static Immersion Test

An immersion test was used to provide quantitative data on the nickel and titanium ions released from specimens. To be able to provide in vitro conditions more aggressive than those in the oral cavity, a solution containing lactic acid, $C_3H_6O_3$, was used (5.85 g L^{-1} NaCl + 10 g L^{-1} lactic acid), pH 2.3. Specimens' surfaces were cleaned ultrasonically in ethanol for 2 min, rinsed with water, and dried with compressed air. Specimens, with dimensions of 40 mm × 7.5 mm, S = 6 cm^2, were immersed in a borosilicate glass test tube (Ø15 mm, 150 mm height) using nylon string with 10 mL of the corrosive solution and clogged with a rubber cork for 7 days at 37 ± 1 °C. The reference solution was held in the same conditions to establish the impurity level for solution elements.

The inductively coupled plasma optical emission spectroscopy (ICP-OES720 device, Agilent, Santa Clara, CA, USA) method was used for quantitative and qualitative elemental analysis of each solution.

2.3.2. Electrochemical Test

For the electrochemical test, the samples with dimensions of 7.5 mm × 7.5 mm and a surface area of 1.125 cm^2 were used. For the measurements, a three-compartment glass cell with a volume of 100 cm^3, a compartment for the saturated calomel reference electrode, and a counter electrode lead wire inserted in the polypropylene bag to avoid hypochlorite formation were used. An electrolyte 9 g L^{-1} NaCl with a pH of 7.4, adjusted with 0.1 M NaOH, was used. Before the polarization measurements, open circuit potentials were simultaneously determined over 2 h with polarization resistance measurements (±10 mV vs. E_{ocp}). For the electrochemical tests, Gamry 1010E potentiostat (Gamry, Warminster, PA, USA) was used.

2.4. Quantitative and Qualitative Analysis of Oxide Layers after Corrosion Testing

To study the oxide layer thickness after the immersion testing and the elemental composition of the coating surface after the electrochemical testing, we used an SEM microscope Quanta 200 3D (FEI, Hillsboro, OR, USA), equipped with a Ga ion source to perform focused ion beam cutting and remove parts of the corrosive layer. The ion milling was performed with an initial platinum deposition on the sample in order to protect the investigated sample surface before performing the cross-section. The cross-section milling depth was 5 µm from the sample surface. After the oxide layer thickness measurements, the chemical content was mapped and analyzed using an energy-dispersive spectroscopeon SEM Sirion 400 NC (FEI, Hillsboro, OR, USA), with an INCA 350 EDS detector (Oxford Instruments, Abingdon, Oxfordshire, UK), using an accelerating voltage of 20 kV.

2.5. Indirect Cytotoxicity Evaluation

NiTi as cast and $NiTi_{cc}$ discs were placed in a tube containing 10 mL of complete medium (DMEM/F12 with 10% FBS and 1% ABAM (all from Gibco, Thermo Fisher, MA, USA), incubated at 37 °C for 2 days, and removed, while the remaining supernatant was used in further experiments. Gingival fibroblast cells were used, as in our previous study [23]. The cells were seeded in a 96-well plate (5.000 cells/well), and the next day 100 µL of supernatant was added to corresponding wells and incubated at 37 °C in a humidified 5% CO_2 atmosphere for up to 7 days. Cells in the complete medium served as a control. The medium was changed every two days. Mitochondrial activity (MTT)

was assessed after 1 and 7 days of treatment. Medium was discarded, medium containing 3-(4,5-dimethylthiazol2-yl)-2,5 diphenyltetrazolium bromide (MTT, 0.5 mg/mL; Sigma Aldrich, St. Louis, MO, USA) was added to each well, and the cells were incubated. After 4 h, supernatant was discarded, and 100 µl DMSO (Sigma Aldrich, St. Louis, MO, USA) was added to each well. Plates were placed on a shaker for 20 min, at 250 rpm, in dark, at 37 °C. Optical density was measured at 550 nm using micro-plate reader RT 2100c (Rayto, Wuxi, China). Values are presented as percentages, calculated as differences to the control group.

3. Results

3.1. Microstructure and ASTM Analysis Results

Optical microscopy images on the 500 µm scale show a predominant equiaxed structure in both samples, but defects and porosity were visible in the matrix of the as-cast sample (Figure 1).

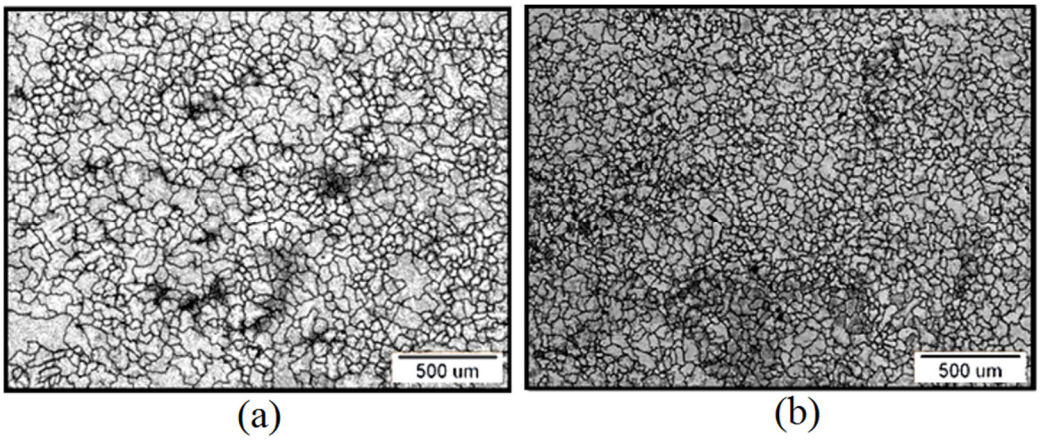

Figure 1. Optical micrography at ×50 magnification: (**a**) NiTi as cast; (**b**) $NiTi_{cc}$.

Table 1 shows the values of the grain number (G) and number of grains per mm^2 and the mean number of intersections for test samples. The average grain size for NiTi as cast was around 50 µm, and that for the $NiTi_{cc}$ the grain size was reduced to values of around 20 µm.

Table 1. Grain size measurement results for NiTi as cast and $NiTi_{cc}$.

Sample	Grain Number (G)	Number of Grains (per mm^2)	Average Grain Size (mm)
NiTi as cast	5	256	0.0527
$NiTi_{cc}$	7	1024	0.0234

3.2. ICP-OES Analysis of the Corrosive Medium after Static Immersion Test

After seven days of immersion in $C_3H_6O_3$ solution, pH 2.3, inductively coupled plasma optical emission spectroscopy analysis showed that the migration of Ni ions was two times higher, and that of Ti was three and a half times higher, in a solution containing NiTi as-cast alloy (Table 2).

Table 2. ICP-OES analysis results in µg cm^{-2} after 7 days of the static immersion test of NiTi as cast and $NiTi_{cc}$ samples in $C_3H_6O_3$ solution, pH 2.3.

Sample	Nickel	Titanium
NiTi as cast	2.33	2.17
$NiTi_{cc}$	1.22	0.631
Reference solution	>0.02	>0.01

Oxide Layer Thickness after Immersion Testing

Figure 2 shows SEM micrographs of focused ion beam cross-sections for NiTi as cast and $NiTi_{cc}$ samples after immersion testing in a $C_3H_6O_3$ solution, pH 2.3. The obtained images indicate that the oxide layer coatings formed on both samples show almost similar thicknesses, but the formed coating on the NiTi as-cast sample (Figure 2b) has a porous and uneven structure.

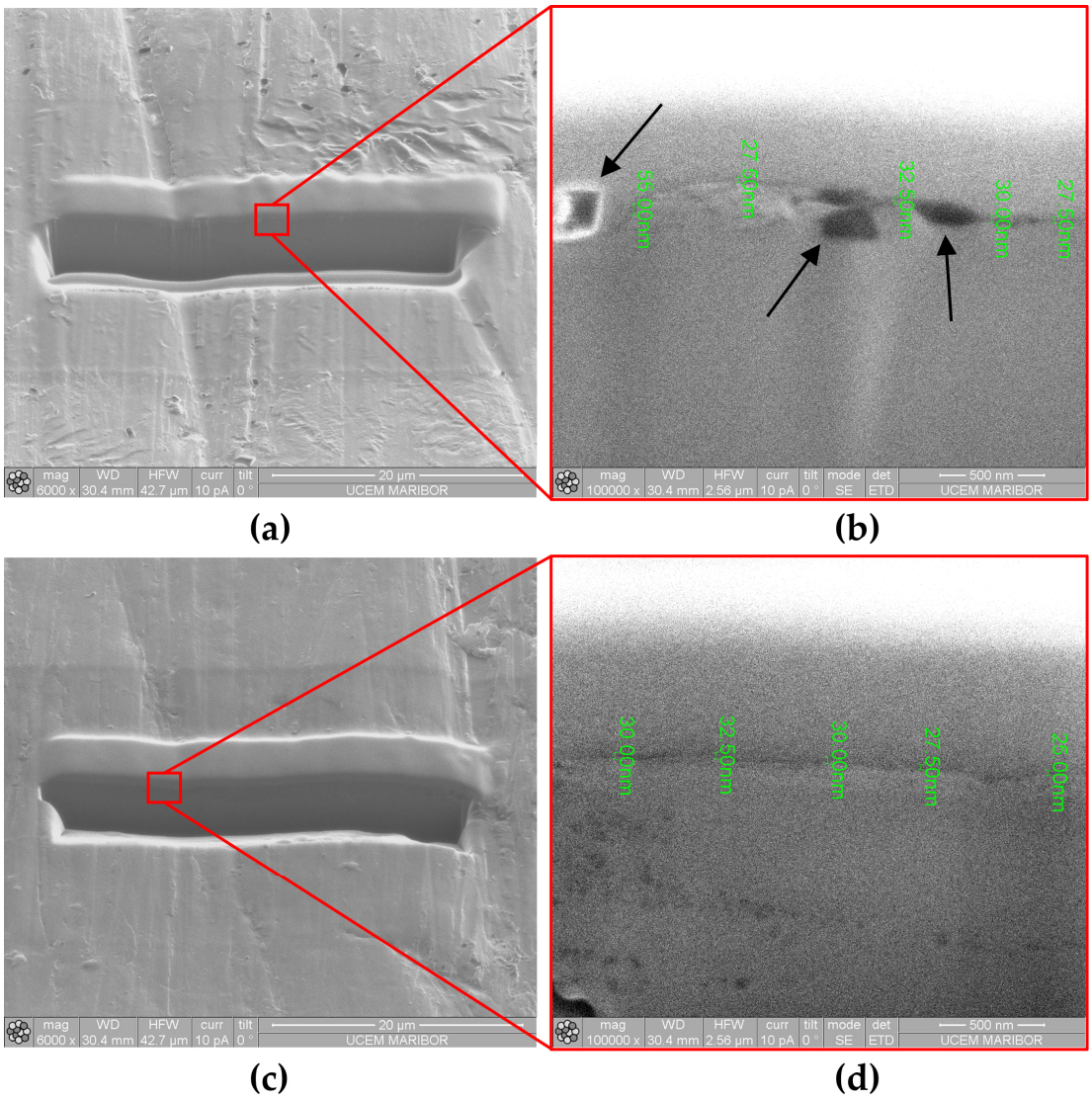

Figure 2. FIB cross-section after immersion testing: (**a**) NiTi as cast, 6000× magnification; (**b**) NiTi as cast, 100,000× magnification. Black arrows indicate defects in the oxide layer; (**c**) $NiTi_{cc}$, 6000× magnification; (**d**) $NiTi_{cc}$, 100,000× magnification.

3.3. Polarization Measurements

Figure 3 shows the dependence of the corrosion potentials over time for NiTi as cast and $NiTi_{cc}$ samples in solution containing 9 g L^{-1} NaCl and with pH = 7.4. NiTi as cast (thermo-mechanical treatment) reached an almost constant negative value E_{corr} of −0.18 V, and $NiTi_{cc}$, without treatment, reached −0.19 V for the same time duration.

The diagram given in Figure 4 represents linear polarization measurements (LPRs) after stabilization of the corrosion potentials of the investigated samples for 2 h. Based on the obtained values, it was demonstrated that $NiTi_{cc}$ has a three-times-higher corrosion polarization resistance in comparison with the NiTi as-cast alloy. The increase in the polar-

ization resistance indicates that the corrosion current density decreased. Moreover, if R_p changes over time, that indicates some surface processes, usually oxide film formation [24].

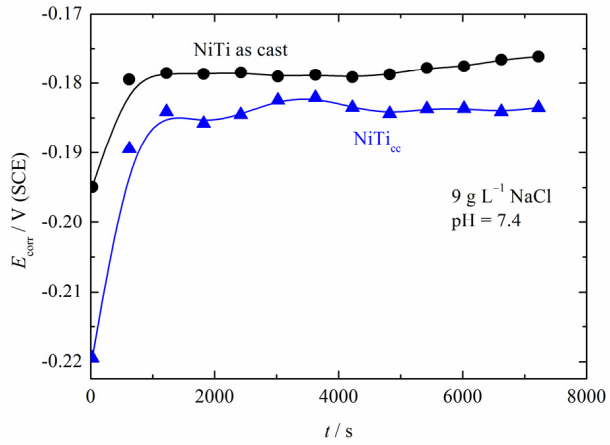

Figure 3. The dependence of the corrosion potential over time for NiTi as cast and NiTi$_{cc}$.

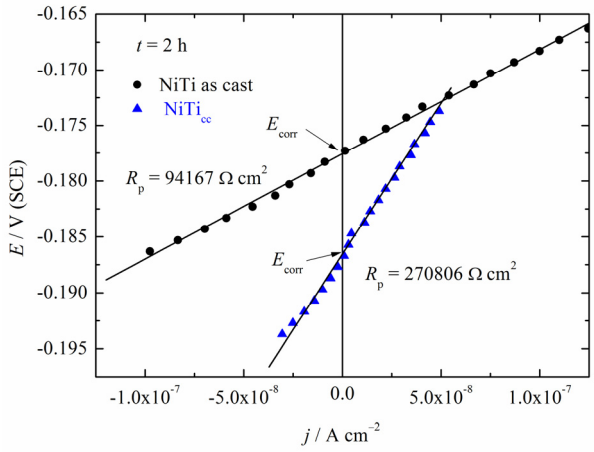

Figure 4. Linear polarization measurements for NiTi as cast and NiTi$_{cc}$ after 2 h of exposure to the corrosive medium, 9 g L^{-1} NaCl.

Figure 5 shows the dependence of the polarization resistance over time. In comparison to NiTi as cast, the polarization resistance, R_p, curve of NiTi$_{cc}$ showed an increase over time, reaching a value of 270 kΩ cm^2 after two hours, while the R_p for NiTi as cast was ~95 kΩ cm^2.

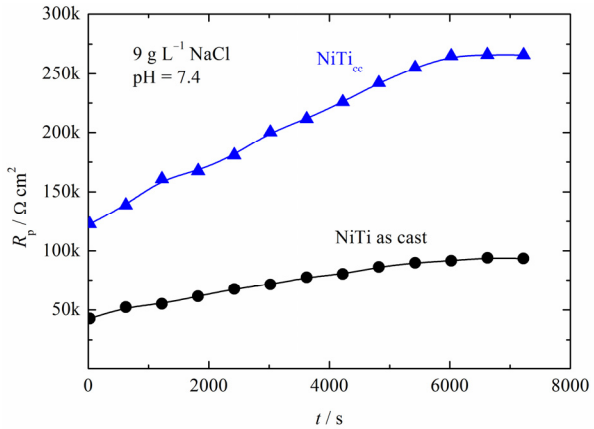

Figure 5. The dependence of R_p over time for NiTi as cast and NiTi$_{cc}$.

The polarization curves of the investigated samples are shown in Figure 6. NiTi, as cast in the anodic direction, practically showed the very narrow potential region of pseudo-passivity followed by active dissolution without Tafel behavior. The slope of the cathodic line was very high, −200 mV dec^{-1}, indicating a complex oxygen reduction reaction probably coupled with changes in the oxide surfaces. The corrosion current density was roughly estimated to be 6 μA cm^{-2}. $NiTi_{cc}$ showed much better corrosion behavior. The cathodic slope was also very high at −188 mV dec^{-1}. A corrosion current density of 0.2 μA cm^{-2} was roughly estimated from the intercept of the cathodic line with the corrosion potential of −0.25 V. Initiation of the passive state started from ~−0.2 V with a passive current density in the range of 0.1 μA cm^{-2}, followed by a metastable pitting region from 0.2 V to 0.37 V, and at ~0.37 V breakdown potential, E_p, or pitting propagation was observed. Considering that differences in the estimated corrosion current densities differ from the determined polarization resistance, we used the modified Stern–Geary equation for the case when the anodic slope tended to infinity:

$$j_{corr} = \frac{|b_c|}{2.3R_p} \quad (1)$$

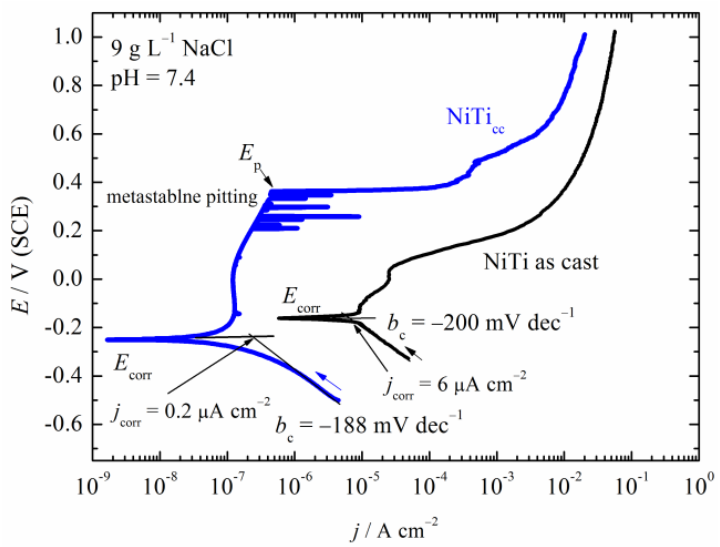

Figure 6. Anodic polarization curve for NiTi as cast and $NiTi_{cc}$ in 9 g L^{-1} NaCl, pH = 7.4, v = 1 mV s^{-1}.

Taking into account that the stationary value of R_p for $NiTi_{cc}$ was 270 kΩ cm^2, while that for NiTi as cast was ~95 kΩ cm^2, the calculated corrosion current densities were 0.32 μA cm^{-2} for $NiTi_{cc}$ and 0.9 μA cm^{-2} for NiTi as cast. For $NiTi_{cc}$, the corrosion current density was in good agreement with the value obtained from polarization measurements, while for that for NiTi as cast was lower. These differences could be connected by the porosity of the film formed onto as-cast NiTi surfaces, which allows a higher corrosion rate under potentiodynamic conditions starting from the cathodic potentials.

Coating Properties (Oxide Layer Thickness and Elemental Analysis) after Polarization Testing

The FIB measurement results demonstrated that NiTi as a cast sample developed almost four times thicker oxide than the $NiTi_{cc}$ sample (Table 3), indicating a more highly corroded surface. Moreover, analyzing the distribution of data representing the numerically expressed values of the depth of the oxide layer for both groups of samples, it was demonstrated that the $NiTi_{cc}$ sample showed more homogeneous data and a lower value of standard deviation (SD = 6.74) in contrast to NiTi as cast (SD = 30).

Figure 7 shows the SEM micrograph and EDX mapping analysis and spectra of the samples after polarization testing.

Table 3. Descriptive statistics of oxide layer thickness (nm) after polarization measurements for NiTi as cast and $NiTi_{cc}$.

	NiTi as Cast	$NiTi_{cc}$
Mean	161.25	44.83
St. Dev.	30	6.74
Min	133.33	33.33
Max	254.17	60
N	20	25

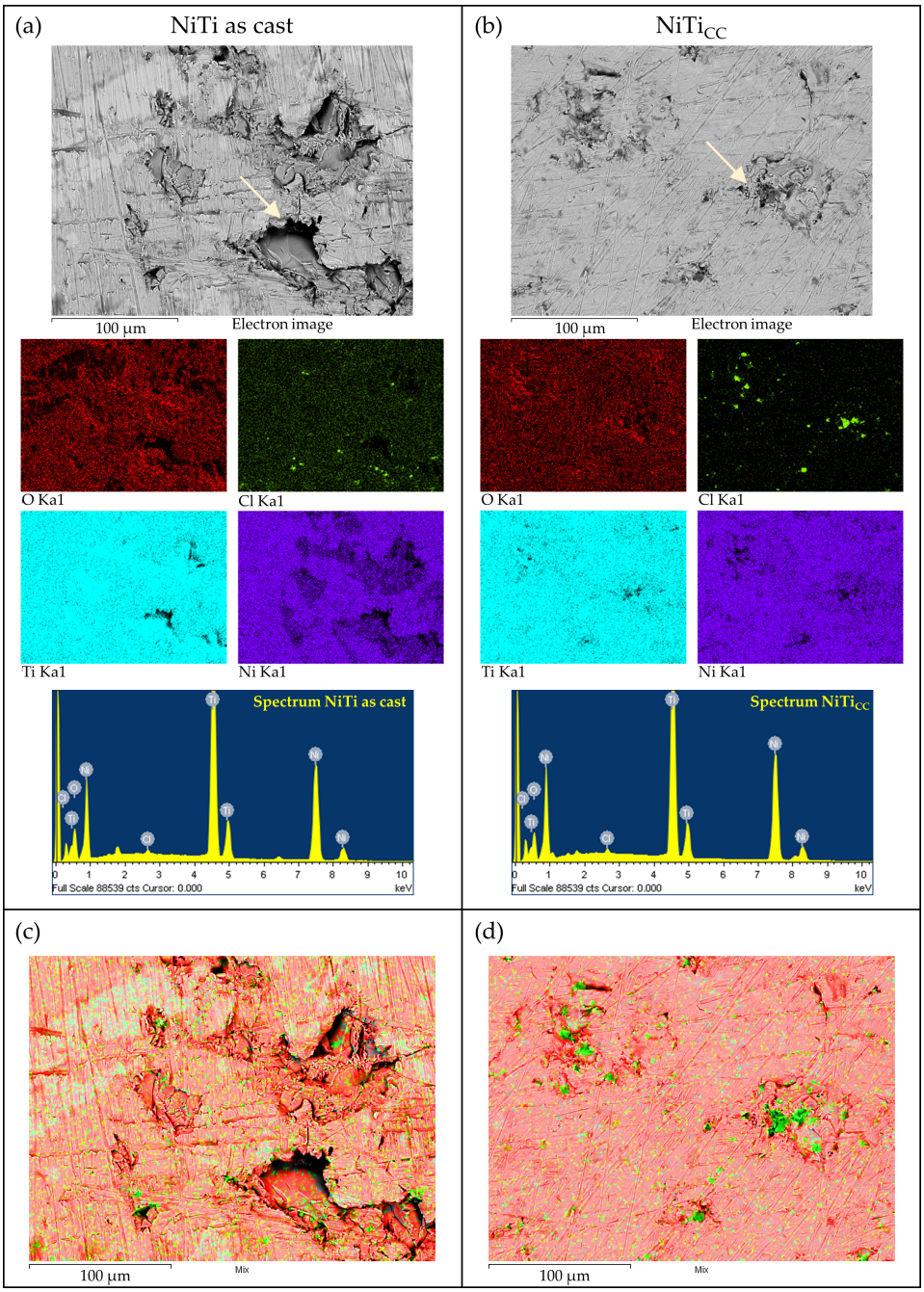

Figure 7. SEM micrographs and EDX mapping of samples after polarization testing: (**a**) NiTi as cast, (**b**) $NiTi_{cc}$. White arrows indicate initiation of pitting corrosion. (**c**) NiTi as cast EDX mapping image of O and Cl content, (**d**) $NiTi_{cc}$ EDX mapping image of O and Cl content. Oxygen is shown in red color, chloride is shown in green color.

The corrosion film formation was substantiated by EDX measurements. The analyzed corroded surfaces of the NiTi samples contained oxygen, titanium, nickel, and small amounts of sodium and chloride. Sodium was removed from the analysis as its elemental mapping and values were correlated with chloride. As seen from the data presented in Figure 7, the Cl presence around the holes on the surfaces of the samples indicated local film breakdown. In sample $NiTi_{cc}$, the Cl was more concentrated around the initiated pitting holes, while in the NiTi as-cast sample, the Cl was also distributed more widely across the sample surface. The initiated pitting holes were also larger, which can be seen as a more advanced local passivity breakdown, as compared to $NiTi_{cc}$. Table 4 shows the weight and atomic percentages of the elements analyzed from the EDX analysis.

Table 4. Results of EDX analysis for coating properties of NiTi samples after polarization test.

Element	Weight%		Atomic%	
	NiTi as Cast	$NiTi_{cc}$	NiTi as Cast	$NiTi_{cc}$
O	16.59	14.16	39.46	35.28
Cl	0.34	0.40	0.37	0.45
Ti	43.22	41.06	34.34	34.16
Ni	39.85	44.37	25.83	30.12

The Cl content was similar in both samples, while the oxygen content was somewhat higher in the NiTi as-cast sample. These results showed a moderately higher amount of corrosion products in the NiTi as-cast sample, composed mainly of Ni and Ti oxides. As mentioned, the Cl ions were more concentrated near the initiated pitting holes, indicating chloride ion penetration through the oxide film.

As an illustration of the corrosion stability of the investigated samples, Figure 8 shows optical and SEM images after anodic polarization. The micrograph of both NiTi as cast and $NiTi_{cc}$, Figure 8b,c and SEM surfaces, Figure 8c,d, shows the presence of localized corrosion attacks on the sample surface present as pits. The diameters of pits on the NiTi as-cast sample ranged from 10 μm to 100 μm, as seen in Figure 8c. The better stability of the $NiTi_{cc}$ sample was obvious because less pits were observed, ranging from a few μm to approximately 50 μm. Accordingly, it seems that $NiTi_{cc}$ was more resistant to pitting corrosion than the NiTi as-cast alloy.

3.4. Cytotoxicity Results

After the first day of exposure, cells' metabolic activity had a mean value of 141% for the solution with molecules from NiTi as cast and 137% for the solution with molecules from the $NiTi_{cc}$ sample, in comparison to the control (Figure 9). Significant metabolic activity was observed under the influence of both materials' extracts. After the seventh day, the mean value of viable cells was 78% for NiTi as cast and 74% for $NiTi_{cc}$. A *t*-test of independent samples showed a statistically significant decrease in cell viability over time for NiTi as cast, $p = 0.017$, and $NiTi_{cc}$, $p = 0.007$. As is known, materials that affect cells' viability to below 70% are considered cytotoxic [25].

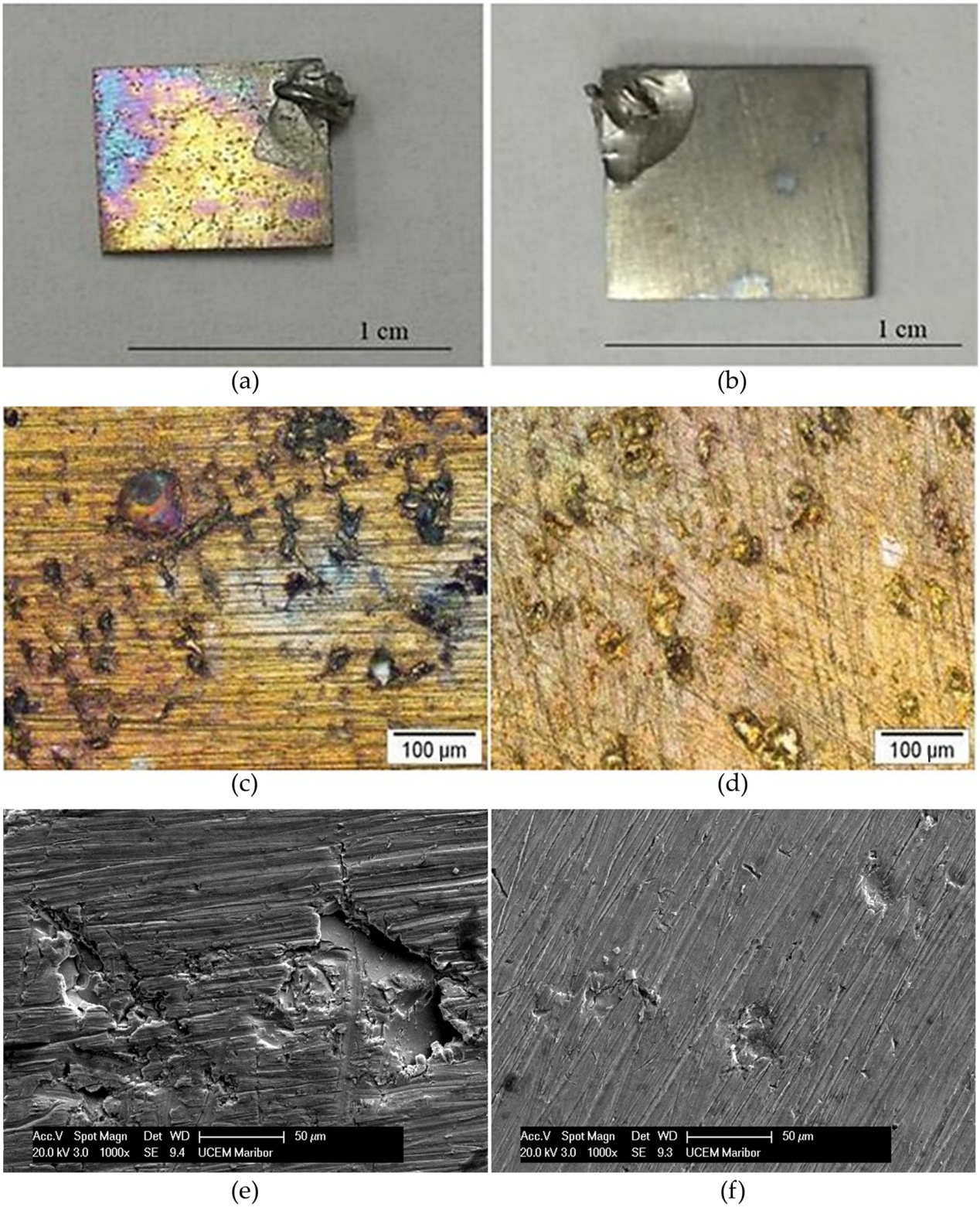

Figure 8. Visual inspection of samples after polarization testing: (**a**) macro view of NiTi as cast; (**b**) macro view of $NiTi_{cc}$; (**c**) optical microscopy of NiTi as cast (200× magnification); (**d**) optical microscopy of $NiTi_{cc}$ (200× magnification); (**e**) electron microscopy of NiTi as cast surface (1000× magnification); (**f**) electron microscopy of $NiTi_{cc}$ (1000× magnification).

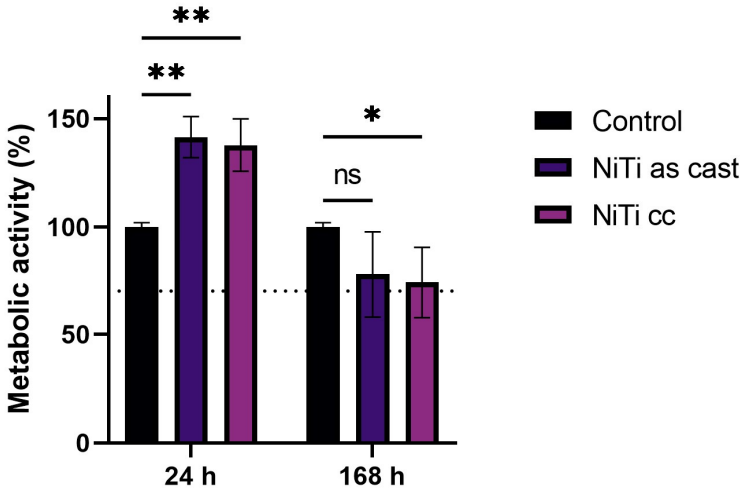

Figure 9. Metabolic activity after 24 h and 168 h of exposure to the materials' extracts. * $p < 0.05$, ** $p < 0.01$, ns $p > 0.05$.

4. Discussion

It is well known that binary NiTi alloys can vary significantly in microstructure parameters depending on the production process [26]. The grain size of each metal material depends on the nucleation centers and the crystal's growth during the solidification of the melt. The higher nickel content in the $NiTi_{cc}$ alloy affected the increase in the number of initial grains during the nucleation process [23,27,28]. The grain size reduction can improve the alloy's superelastic properties, as it allows the desired orientation and stability of formatted grains due to the possibility of producing a larger number of martensite plates [29]. Moreover, it is known that grain refinement substantially enhances ductility.

The investigation of the microstructure and surface morphology before corrosion tests revealed defects and porosity which were initiation sites for pitting corrosion of the NiTi as-cast alloy. Still, the NiTi alloy has some applications in the cast condition [20].

The clinical implication of in vitro corrosion tests is in analytical measurements of the released metal ions that can lead to adverse toxicological effects. An immersion test conducted for seven days showed that the elevated Ni content released from an acidic environment exceeded the safety limit for both groups of samples. According to European Directive 2004/96/EC, allowable limits for humans are 0.2 $\mu g\ cm^{-2}$ [30]. However, Ni ion release from the $NiTi_{cc}$ sample is two times lower.

It is well documented that the most common adverse reactions that occur due to metal dissolution from nitinol devices in the oral cavity are burning mouth syndrome and oral lichenoid reactions. Those symptoms are manifestations of delayed allergy reactions (type IV), and nickel is known to be the allergen with the highest frequency related to this clinical complaint [31].

The potential corrosion values for the investigated alloys were negative. Keeping in mind that positive potentials in the oral cavity could in some cases correspond to a polarization value of 300–400 mV [24], it is evident that NiTi as cast showed unsatisfactory results. The anodic curve for NiTi as cast showed practically only active anodic dissolution. This could be connected by the more porous oxide film formed on the NITi as cast surface. Similar results were obtained for the sintered NiTi with the addition of Cu and Nb [32]. For the $NiTi_{cc}$ alloy, after the passive region, the current density fluctuations in the anodic curve were recognized as a region of metastable pitting. Relatively narrow, stable passive regions indicated the possible susceptibility to pitting corrosion in some cases. Most of the authors agree that the passive layer expanded over the entire alloy surface, and XPS revealed that the layer was composed mainly of TiO_2, Ti_2O_3, and a small amount of TiO and prevented Ni dissolution from the surface [33]. Figure 10 represents simplified corrosion processes of the investigated alloys under anodic polarization. For NiTi as cast, a thick layer was formed

and could be considered porous, because no passivation was observed. Ti^{4+} ions could diffuse through pores and, with oxygen and OH^- ions, form TiO_2 and precipitate onto the oxide surface. For relatively small Ni^{2+} concentrations, critical pH for the precipitation of $Ni(OH)_2$ is, according to the Pourbaix diagram, around nine; consequently, Ni^{2+} ions probably diffuse into solutions. A decrease in the Ni surface concentration was observed by EDX, as shown in Table 4.

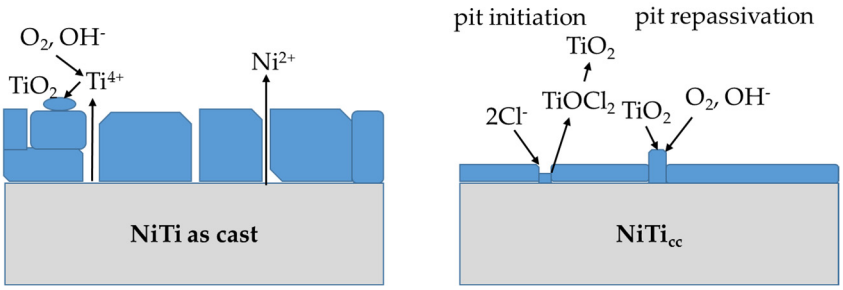

Figure 10. Simplified schematic presentation of the corrosion processes under anodic polarization of NiTi as cast and $NiTi_{cc}$.

The $NiTi_{cc}$ showed a passive region, so during passivity and metastable pitting, the corrosion process could be as follows.

When Cl^- ions reach the oxide film/solution interface, in the case of the amorphous structure of oxide, and regarding the small diameter of this molecule, they will quickly adsorb [34]. In the reaction with TiO_2, unstable soluble titanium oxychloride, $TiOCl_2$, is formed, diffused into the solution, and hydrolyzed to TiO_2. Consequently, by penetration, the oxide film becomes thinner, which is known as pit initiation. These atomic defects present a local thinning mechanism [35]. Because competition between chloride and oxygen or water adsorption in the passive region exists, the formed pits could be repassivated [36]. After the breakdown potential, the corrosion mechanism becomes similar to that in the case of the NiTi as-cast alloy.

By evaluating the comprehensive results of the corrosion tests, it poor corrosion resistance of the as-cast alloy and better stability of the continuously cast alloy were recorded. However, the lower corrosion stability of NiTi as cast compared to that of $NiTi_{cc}$ indicates that structural changes caused by the machining of the classically cast alloy also contributed to this. The smaller grains within the $NiTi_{cc}$ alloy may be the reason for its better corrosion properties.

Indirect contact involves simultaneous analysis of only corrosion effect products (metal ions and/or newly formed compounds) that were released from the alloys into the cell medium culture through inhomogeneous parts of the oxide. As shown in a previous study, the cytotoxicity of the NiTi extracts is strongly correlated to the oxidative stress that occurs in the cells [37,38]. Initially, in the first 24 h cell metabolic activity was significantly raised in the presence of materials' extracts, probably affected by metal ions in the medium, while in a prolonged time period, the metabolic activity dropped below that of the control cells, but still remained above 70%. The enhanced metabolic activity of fibroblasts was shown to be transitory.

The results of our study are in agreement with recently reported evidence that human lung fibroblasts displayed altered cell signaling when indirectly exposed to nitinol alloys [39]. The Ni^{2+} ions released from the alloy increased free radical production in cells, suggesting metal toxicity. The scientific literature is poor, with evidence of indirect biocompatibility of the nitinol alloy. On the contrary, several studies indicate good biocompatibility of nickel–titanium in direct tests, showing that different cell lines can proliferate on alloys' surfaces [23,40]. From the perspective of passive alloys, direct contact means cells adhered to Ti and Ni oxides, depending on the weight percentage surface ratio. It is well documented that Ti oxides exert bioactive characteristics. According to the literature

data, oxides on the alloy surface will occur when an alloy is immersed in a cell culture medium with a pH-neutral value [4].

In correlation with the cytological characterization of the oral cavity, for in vitro cytotoxicity testing of alloys, primary fibroblast cell lines were selected. Fibroblasts are present in almost all tissue types and are essential in inflammatory tissue reactions. Also, these cells are among the first to be detected within a healing surgical wound [41].

But, differences between in vivo and in vitro conditions are numerous. In the case of nickel toxicity evaluation, laboratory conditions can be clinically irrelevant [42]. Primarily, controlled conditions for cell cultivation do not allow their metabolic activity to be as it is inside a living organism. Second, cell culture media are pH-neutral suspensions. They may be irrelevant to the degradation resistance of some metallic materials. In vivo, the conditions are characterized by changes in the acid–base balance. For example, during implant placement, the pH value in the surgical site decreases up to 5.5. Recovery towards neutral values takes two weeks [43]. Local acidity significantly impacts nickel ion leaching. Third, during the clinical implantation of metallic materials, the transport of released metal ions may occur in distant tissues and organs and lead to interactions that are impossible to predict.

5. Conclusions

Based on the obtained results, the following was subsequently observed:

- The method of continuous casting can improve a material's microstructure along with the corrosion resistance. Better surface stability reduces the Ni ion release.
- Continuous-cast alloys showed better protective characteristics of the surface oxide layer in comparison to commercial NiTi alloys.
- The corroded surface of the NiTi as-cast sample developed thicker oxides with uneven structures, leading to three-times-higher Ni ion release.
- High corrosion density and low corrosion potential indicated low corrosion resistance for the NiTi as-cast sample. Pitting corrosion occurred with pits in diameters up to 100 μm.
- $NiTi_{cc}$ showed much better corrosion properties than NiTi as-cast alloys.
- Ni ions released in the conditioning cell mediums of both samples led to a statistically significant decrease in cell viability over seven days.

Author Contributions: Conceptualization, B.N.G. and M.M.L.; methodology, B.N.G., M.M.L., P.M. and D.M.; software, K.R.; validation, B.N.G., R.R. and I.Đ.; formal analysis, K.R.; investigation, M.M.L.; resources, B.N.G., P.M. and I.Đ.; data curation, B.N.G. and R.R.; writing—original draft preparation, M.M.L. and B.N.G.; writing—review and editing, B.N.G., R.R., D.M. and I.Đ.; visualization, M.M.L.; supervision, B.N.G.; project administration, R.R.; funding acquisition, B.N.G. All authors have read and agreed to the published version of the manuscript.

Funding: This research was funded by the International Eureka project GOLD-GERE!17091.

Institutional Review Board Statement: The study, conducted in accordance with the Declaration of Helsinki, was reviewed and approved by the institutional Ethical Committee (approval number 36/7).

Data Availability Statement: The data presented in this study are available on request from the corresponding author. The data are not publicly available due to confidentiality.

Conflicts of Interest: The authors declare no conflicts of interest.

References

1. Eliaz, N. Corrosion of Metallic Biomaterials: A Review. *Materials* **2019**, *12*, 407. [CrossRef] [PubMed]
2. Almeraya-Calderón, F.; Jáquez-Muñoz, J.M.; Maldonado-Bandala, E.; Cabral-Miramontes, J.; Nieves-Mendoza, D.; Olgui-Coca, J.; Lopez-Leon, L.D.; Estupiñán-López, F.; Lira-Martínez, A.; Gaona Tiburcio, C. Corrosion Resistance of Titanium Alloys Anodized in Alkaline Solutions. *Metals* **2023**, *13*, 1510. [CrossRef]
3. Ibrahim, H.; Jahadakbar, A.; Dehghan, A.; Moghaddam, N.S.; Amerinatanzi, A.; Elahinia, M. In Vitro Corrosion Assessment of Additively Manufactured Porous NiTi Structures for Bone Fixation Applications. *Metals* **2018**, *8*, 164. [CrossRef]

4. Ryhänen, J.; Niemi, E.; Serlo, W.; Niemelä, E.; Sandvik, P.; Pernu, H.; Salo, T. Biocompatibility of nickel-titanium shape memory metal and its corrosion behavior in human cell cultures. *J. Biomed. Mater. Res.* **1997**, *35*, 451–457. [CrossRef]
5. Cioffi, M.; Gilliland, D.; Ceccone, G.; Chiesa, R.; Cigada, A. Electrochemical release testing of nickel-titanium orthodontic wires in artificial saliva using thin layer activation. *Acta Biomater.* **2005**, *1*, 717–724. [CrossRef] [PubMed]
6. Taqa, A.; Fathi, W.; Mohammed, R. Evaluation of Nickel Ion Release from Orthodontic Wires in Different Types of Artificial Saliva. *Al-Rafidain Dent. J.* **2014**, *14*, 182–188. [CrossRef]
7. Lee, T.-H.; Huang, T.-K.; Lin, S.-Y.; Chen, L.-K.; Chou, M.-Y.; Huang, H.-H. Corrosion Resistance of Different Nickel-Titanium Archwires in Acidic Fluoride-containing Artificial Saliva. *Angle Orthod.* **2010**, *80*, 547–553. [CrossRef]
8. Pound, B. Susceptibility of nitinol to localized corrosion. *J. Biomed. Mater. Res. Part A* **2006**, *77*, 185–191. [CrossRef]
9. Frankel, G.S.; Li, T.; Scully, J.R. Perspective—Localized corrosion: Passive film breakdown vs pit growth stability. *J. Electrochem. Soc.* **2017**, *164*, C180–C181. [CrossRef]
10. Sharma, S.; Hashmi, M.F. Partial Pressure of Oxygen. In *StatPearls*; StatPearls Publishing: Treasure Island, FL, USA, 2023.
11. Beetham, R. Scientific Committee of the Association of Clinical Biochemists A Review of Blood pH and Blood-Gas Analysis. *Ann. Clin. Biochem.* **1982**, *19*, 198–213. [CrossRef]
12. Farber, E.; Orlov, A.; Borisov, E.; Repnin, A.; Kuzin, S.; Golubkov, N.; Popovich, A. TiNi Alloy Lattice Structures with Negative Poisson's Ratio: Computer Simulation and Experimental Results. *Metals* **2022**, *12*, 1476. [CrossRef]
13. Ding, Z.; Zhao, J.; Misra, R.D.K.; Guo, F.; Xie, Z.; Wang, X.; Li, X.; Wang, J.; Shang, C. Deep Learning-Based Understanding of Defects in Continuous Casting Product. *Metals* **2023**, *13*, 1809. [CrossRef]
14. Mohammadi, Z.; Soltani, M.K.; Shalavi, S.; Asgary, S. A Review of the Various Surface Treatments of NiTi Instruments. *Iran. Endod. J.* **2014**, *9*, 235–240. [PubMed]
15. Sullivan, S.J.L.; Dreher, M.L.; Zheng, J.; Chen, L.; Madamba, D.; Miyashiro, K.; Trépanier, C.; Nagaraja, S. Effects of Oxide Layer Composition and Radial Compression on Nickel Release in Nitinol Stents. *Shap. Mem. Superelast.* **2015**, *1*, 319–327. [CrossRef]
16. Shabalovskaya, S.A.; Anderegg, J.; Laab, F.; Thiel, P.A.; Rondelli, G. Surface conditions of Nitinol wires, tubing, and as-cast alloys. The effect of chemical etching, aging in boiling water, and heat treatment. *J. Biomed. Mater. Res. B Appl. Biomater.* **2003**, *65*, 193–203. [CrossRef] [PubMed]
17. Clarke, B.; Carroll, W.; Rochev, Y.; Hynes, M.; Bradley, D.; Plumley, D. Influence of Nitinol wire surface treatment on oxide thickness and composition and its subsequent effect on corrosion resistance and nickel ion release. *J. Biomed. Mater. Res.* **2006**, *79A*, 61–70. [CrossRef] [PubMed]
18. Trepanier, C.; Venugopalan, R.; Pelton, A.R. Corrosion Resistance and Biocompatibility of Passivated NiTi. In *Shape Memory Implants*; Yahia, L., Ed.; Springer: Berlin/Heidelberg, Germany, 2000; pp. 35–45, ISBN 978-3-642-64118-3.
19. Shabalovskaya, S.; Anderegg, J.; Van Humbeeck, J. Critical overview of Nitinol surfaces and their modifications for medical applications. *Acta Biomater.* **2008**, *4*, 447–467. [CrossRef] [PubMed]
20. Elshaer, R.N.; Ibrahim, K.M. Study of Microstructure, Mechanical Properties, and Corrosion Behavior of As-Cast Ni-Ti and Ti-6Al-4V Alloys. *J. Mater. Eng. Perform.* **2023**, *32*, 7831–7845. [CrossRef]
21. Lojen, G.; Stambolić, A.; Šetina Batič, B.; Rudolf, R. Experimental Continuous Casting of Nitinol. *Metals* **2020**, *10*, 505. [CrossRef]
22. Stambolić, A.; Jenko, M.; Kocijan, A.; Žužek, B.; Drobne, D.; Rudolf, R. Determination of mechanical and functional properties by continuous vertical cast NiTi rod. *Mater. Tehnol.* **2018**, *52*, 521–527. [CrossRef]
23. Miličić Lazić, M.; Majerič, P.; Lazić, V.; Milašin, J.; Jakšić, M.; Trišić, D.; Radović, K. Experimental Investigation of the Biofunctional Properties of Nickel–Titanium Alloys Depending on the Type of Production. *Molecules* **2022**, *27*, 1960. [CrossRef] [PubMed]
24. Iacoban, S.; Mareci, D.; Bolat, G.; Munteanu, C.; Souto, R.M. Multiscale Electrochemical Investigation of the Corrosion Resistance of Various Alloys Used in Dental Prostheses. *Metall. Mater. Trans. B* **2015**, *46*, 1011–1021. [CrossRef]
25. Cannella, V.; Altomare, R.; Chiaramonte, G.; Di Bella, S.; Mira, F.; Russotto, L.; Pisano, P.; Guercio, A. Cytotoxicity Evaluation of Endodontic Pins on L929 Cell Line. *BioMed Res. Int.* **2019**, *2019*, 3469525. [CrossRef]
26. Clemens, H.; Mayer, S.; Scheu, C. Microstructure and Properties of Engineering Materials. In *Neutrons and Synchrotron Radiation in Engineering Materials Science*; John Wiley & Sons, Ltd.: Hoboken, NJ, USA, 2017; pp. 1–20, ISBN 978-3-527-68448-9.
27. Feng, Y.; Du, Z.; Hu, Z. Study on the Effect of Ni Addition on the Microstructure and Properties of NiTi Alloy Coating on AISI 316 L Prepared by Laser Cladding. *Materials* **2021**, *14*, 4373. [CrossRef]
28. Mashreghi, A.; Zare, H. Investigation of nucleation and growth mechanism during electrochemical deposition of nickel on fluorine doped tin oxide substrate. *Curr. Appl. Phys.* **2016**, *16*, 599–604. [CrossRef]
29. Elahinia, M.; Shayesteh Moghaddam, N.; Taheri Andani, M.; Amerinatanzi, A.; Bimber, B.A.; Hamilton, R.F. Fabrication of NiTi through additive manufacturing: A review. *Prog. Mater. Sci.* **2016**, *83*, 630–663. [CrossRef]
30. Commission Directive 2004/96/EC of 27 September 2004 Amending Council Directive 76/769/EEC as Regards Restrictions on the Marketing and Use of Nickel for Piercing Post Assemblies for the Purpose of Adapting Its Annex I to Technical Progress (Text with EEA Relevance). Available online: https://www.legislation.gov.uk/eudr/2004/96/contents (accessed on 20 August 2023).
31. Baričević, M.; Mravak-Stipetić, M.; Stanimirović, A.; Blanuša, M.; Kern, J.; Lončar, B.; Andabak, A.; Baričević, D. Salivary concentrations of nickel and chromium in patients with burning mouth syndrome. *Acta Dermatovenerol. Croat.* **2011**, *19*, 2–5.
32. Lethabane, M.L.; Olubambi, P.A.; Chikwanda, H.K. Corrosion behaviour of sintered Ti–Ni–Cu–Nb in 0.9% NaCl environment. *J. Mater. Res. Technol.* **2015**, *4*, 367–376. [CrossRef]

33. Hu, T.; Chu, C.; Xin, Y.; Wu, S.; Yeung, K.W.K.; Chu, P.K. Corrosion products and mechanism on NiTi shape memory alloy in physiological environment. *J. Mater. Res.* **2010**, *25*, 350–358. [CrossRef]
34. Parangusan, H.; Bhadra, J.; Al-Thani, N. A review of passivity breakdown on metal surfaces: Influence of chloride- and sulfide-ion concentrations, temperature, and pH. *Emergent Mater.* **2021**, *4*, 1187–1203. [CrossRef]
35. Marcus, P.; Maurice, V.; Strehblow, H.-H. Localized corrosion (pitting): A model of passivity breakdown including the role of the oxide layer nanostructure. *Corros. Sci.* **2008**, *50*, 2698–2704. [CrossRef]
36. Asserghine, A.; Filotás, D.; Nagy, L.; Souto, R.M.; Nagy, G. Do titanium biomaterials get immediately and entirely repassivated? A perspective. *Npj Mater. Degrad.* **2022**, *6*, 57. [CrossRef]
37. Rincic Mlinaric, M.; Durgo, K.; Katic, V.; Spalj, S. Cytotoxicity and oxidative stress induced by nickel and titanium ions from dental alloys on cells of gastrointestinal tract. *Toxicol. Appl. Pharmacol.* **2019**, *383*, 114784. [CrossRef] [PubMed]
38. Marchenko, E.; Baigonakova, G.; Dubovikov, K.; Kokorev, O.; Yasenchuk, Y.; Vorozhtsov, A. In Vitro Bio-Testing Comparative Analysis of NiTi Porous Alloys Modified by Heat Treatment. *Metals* **2022**, *12*, 1006. [CrossRef]
39. Pouwels, S.D.; Sigaeva, A.; de Boer, S.; Eichhorn, I.A.; Koll, L.; Kuipers, J.; Schirhagl, R.; Heijink, I.H.; Burgess, J.K.; Slebos, D.-J. Host–device interactions: Exposure of lung epithelial cells and fibroblasts to nickel, titanium, or nitinol affect proliferation, reactive oxygen species production, and cellular signaling. *J. Mater. Sci. Mater. Med.* **2023**, *34*, 38. [CrossRef] [PubMed]
40. Chrzanowski, W.; Neel, E.A.A.; Armitage, D.A.; Zhao, X.; Knowles, J.C.; Salih, V. In vitro studies on the influence of surface modification of Ni-Ti alloy on human bone cells. *J. Biomed. Mater. Res. A* **2010**, *93*, 1596–1608. [CrossRef]
41. Bainbridge, P. Wound healing and the role of fibroblasts. *J. Wound Care* **2013**, *22*, 407–412. [CrossRef]
42. Balać, I.; Bugarski, B.; Ćosić, I.; Dramićanin, M.; Đorđević, D.; Filipović, N.D.; Ignjatović, N.L.; Janaćković, Đ.T.; Kojić, M.; Manojlović, V.; et al. *Biomaterijali*; Materials Research Society, Institute of Technical Sciences of the Serbian Academy of Sciences and Art: Belgrade, Serbia, 2010; ISBN 978-86-80321-23-3.
43. Mani, G.; Porter, D.; Grove, K.; Collins, S.; Ornberg, A.; Shulfer, R. Surface finishing of Nitinol for implantable medical devices: A review. *J. Biomed. Mater. Res. B Appl. Biomater.* **2022**, *110*, 2763–2778. [CrossRef]